

LETTER TO THE EDITOR

First detection of a minor merger at $z \sim 0.6$

M. Puech^{1,2}, F. Hammer², H. Flores², B. Neichel², Y. Yang², and M. Rodrigues²

¹ ESO, Karl-Schwarzschild-Strasse 2, D-85748 Garching bei München, Germany

² GEPI, Observatoire de Paris, CNRS, University Paris Diderot; 5 Place Jules Janssen, 92190 Meudon, France

Received...accepted...

ABSTRACT

Context. Numerical simulations predict that minor mergers are an important channel for the mass assembly of galaxies. However, minor mergers are relatively difficult to detect using imaging, especially at high redshift. While such events are much less violent than major mergers, they can nevertheless leave several features on the kinematical structures of remnant galaxies which could be detected using 3D spectroscopy.

Aims. We present the first direct detection of a minor merger in a $z \sim 0.6$ galaxy. Such events could indeed be good candidates to explain the kinematics of perturbed rotating disks observed with GIRAFFE at $z \sim 0.6$.

Methods. We present photometric and kinematical evidence of such an event in a combined analysis of three-band HST/ACS imaging and VLT/GIRAFFE 2D-kinematics.

Results. Using these data, we are able to demonstrate that a minor merger of a relatively small satellite (mass ratio $\sim 1:18$) is occurring in this galaxy. We also derive a total SFR of $\sim 21 M_{\odot}/yr$.

Conclusions. Minor mergers could be one of the physical processes explaining the kinematics of perturbed rotating disks, which represent $\sim 25\%$ of emission line intermediate mass galaxies at $z \sim 0.6$. 3D spectroscopy appears to be a very good tool to identify minor mergers in distant (and local) galaxies.

Key words. Galaxies: evolution; Galaxies: kinematics and dynamics; Galaxies: high-redshifts; galaxies: general; galaxies: interactions; galaxies: spiral.

1. Introduction

Minor mergers are usually defined as the merging between two galaxies with a mass ratio smaller than 1:3 to 1:5. Hence, during a single minor merger event, the amount of stellar mass added to the main progenitor remains negligible. However, cosmological simulations predict that minor mergers are one order of magnitude more frequent than major mergers (e.g., Khochfar & Silk 2006); Moreover, they can be responsible for *in situ* star formation episodes (Woods et al. 2006; Woods & Geller 2007) during the interaction. Therefore, minor mergers are thought to be an important channel for the galaxy mass assembly, even possibly the dominant contributor for intermediate mass galaxies (Guo & White 2007).

Contrary to major mergers, minor mergers are much less violent dynamical processes since they do not destroy the disk of the main progenitor. Nevertheless, minor mergers can result in several important imprints on the morphological and kinematical structure of the remnant: they can thicken the disk of the main progenitor by increasing its vertical scale-length and velocity dispersion, as found both in numerical simulations (Toth & Ostriker 1992; Walker et al. 1996; Velazquez & White 1999; Bournaud et al. 2005; Robertson et al. 2006) and observations (Schwarzkopf & Dettmar 2000). They are believed to play an important role during the formation of thick disks (e.g., Yoachim & Dalcanton 2006), and they could also explain several other structural properties of spiral galaxies, such as the formation of anti-truncated surface brightness profiles (Younger et al. 2007), or activation of bars (Laine & Heller 1999).

In spite of their possible cosmological importance and influence on galaxy structure, relatively few studies have focused on minor mergers. Statistical studies aiming at identifying an important number of minor mergers in large photometric surveys rely on counts of galaxies in pairs which have a large difference in a red band magnitude, used as a proxy for the stellar mass. One of the main difficulty encountered is then the high frequency of false pairs due to the large number of background galaxies, which makes it necessary to have spectroscopic confirmations for both progenitors (Woods et al. 2006). Moreover, once the minor progenitor gets too close to the main progenitor, it becomes difficult to separate both objects using imaging alone, especially at high redshift. Therefore, detailed studies of minor mergers are quite rare (Laine & Heller 1999).

Another route for identifying on-going minor mergers may be to use 3D spectroscopy. Using GIRAFFE at the VLT, Yang et al. (2007) studied the 2D-kinematical properties of a complete sample of 63 $z \sim 0.6$ galaxies, which are representative of $M_{\text{stellar}} \geq 1.5 \cdot 10^{10} M_{\odot}$ emission line ($EW_0([OII]) \geq 15 \text{ \AA}$) galaxies. Interestingly, they have classified 25% of these objects as “perturbed rotating” galaxies (PR): their kinematics shows all the features of a rotating disk, but with a peak in the velocity dispersion map shifted away from the dynamical center. These local perturbations cannot be reproduced from the rotation patterns, and thus cannot be attributed to rotation (Yang et al. 2007). They might illustrate a possible minor merger event, which does not affect the disk stability, but has an expected signature in the σ map.

Other studies have also revealed the existence of morphologically and/or kinematically disturbed galaxies at higher redshifts.

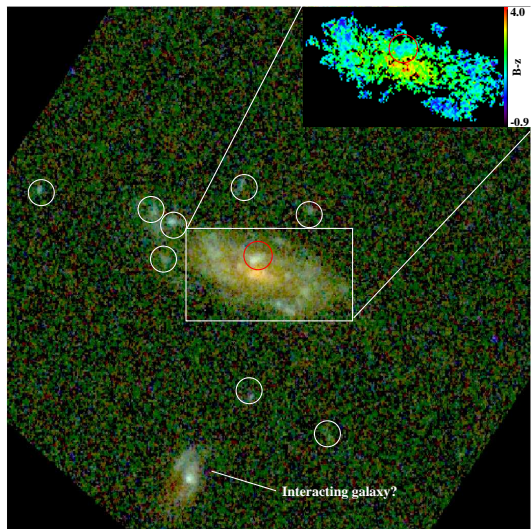


Fig. 1. Three bands HST/ACS imaging of J033226.23-274222.8 (~ 0.03 arcsec/pix). The B band is coded in blue, the V band in green, and the z band in red. The FoV is 16×16 arcsec²; North is up, East is left. The contrast has been optimized by hand. White circles indicate the position of low surface brightness debris. The position of the infalling satellite is indicated by a red circle. *Upper-right Inset:* B-z color map of J033226.23-274222.8 from HST/ACS imaging. The FoV is a $\sim 4.3 \times 2.5$ arcsec² zoom on J033226.23-274222.8.

Förster-Schreiber et al. (2006) have obtained 3D spectroscopy of several $z \sim 2$ galaxies among which some also show off-centered σ peaks in relatively well-ordered VFs. However, all these studies (including GIRAFFE) are seeing limited, and the physical process responsible for such off-centered σ peaks remains unclear, even when using adaptive optics (Law et al. 2007). In this *letter*, we present what is, to our knowledge, the first direct evidence for the detection of a minor merger at high redshift. This object (J033226.23-274222.8) has been classified as a PR by Yang et al. (2007) and is thus an ideal case to test the possibility that minor mergers could be a viable process explaining PR kinematics. This *letter* is organized as follows: Sect. 1 presents the general properties of J033226.23-274222.8; Sect. 2 details the kinematical evidences for a minor merger event in this galaxy; Sect. 3 gives some estimates for the mass and the star formation rate; A conclusion is given in Sect. 4. We adopt $H_0 = 70$ km/s/Mpc, $\Omega_M = 0.3$, and $\Omega_\Lambda = 0.7$, and the AB magnitude system.

2. General properties

In Fig. 1, we show a B-V-z composite HST/ACS image, which presents an extended view of J033226.23-274222.8. J033226.23-274222.8 is a late-type spiral galaxy with a small red central bulge ($B/T = 0.05$) and an extended disk (half light radius $R_{half} = 9.47$ kpc, see Neichel et al. 2007). One can note another galaxy located ~ 5 arcsec SSE: unfortunately, we were not able to retrieve any valuable redshift information for this galaxy, but the presence of a lot of debris surrounding J033226.23-274222.8 suggests that these two galaxies might be in the first stage of an interaction.

The B-z color map (see inset in Fig. 1) reveals a central small bulge with a color similar to that of a passively evolved E/S0 galaxy, as well as several small (~ 1 kpc) blue regions located in the disk outskirts; they have colors consistent with star-bursting regions (see Neichel et al. 2007 for details), which suggests a

progressive inside-out build-up of the disk. At the North side of the bulge, one can note a more extended (~ 2 kpc) blue region (see the red circle). This region shows a tail oriented close to West, and is significantly redder and larger than other HII regions, which favors the idea that this region is a small infalling satellite, rather than another HII region. We suspect that this satellite is part of the system of blue debris surrounding J033226.23-274222.8, which would be infalling onto it with a trajectory as suggested by the orientation of the tail.

3. Kinematical evidence for a minor merger

In Fig. 2, we have superimposed the VF and the σ -map derived from GIRAFFE observations (Yang et al. 2007) on the B-V-z composite ACS image. Aligning ground-based IFU data with space imaging requires accurate astrometries. In ACS images, astrometry is derived using the GSC2 catalog, with a residual rms uncertainty on both Ra and Dec of 0.12 arcsec¹. On the other hand, GIRAFFE observations are prepared using the USNO catalog (see Flores et al. 2006). During observations, 4 FACB stars are used to align the GIRAFFE plate (where IFUs are positioned), with the sky coordinate system: systematic offsets between the USNO catalog and the observational system are then minimized. The random residual error on this correction is estimated to be less than 0.15 arcsec rms (Pasquini et al. 2004). Using Skycat on the original z-band large field image (corresponding to the GOODS section #34), we picked astrometry for the 11 stars common to both GSC2 and USNO catalogs. We used them to derive the mean offset between the two catalogs, and correct the position of the IFU relative to ACS images: this correction is ~ 0.11 arcsec in RA, and ~ 0.04 arcsec in Dec. Combining the rms residual uncertainties from both catalogs, we derive a conservative ~ 0.23 arcsec residual random uncertainty on the position of the IFU relative to ACS images (see the scale-bars in the bottom-left corners), i.e., close to half a GIRAFFE pixel (0.52 arcsec/pix).

Figure 2 shows a regular VF with no apparent perturbations, especially close to the infalling satellite. However, given the limited spatial resolution of GIRAFFE, only very large-scale deviations are detectable and we cannot exclude the presence of non-detected small scale perturbations in the VF. We have measured the photometric PA using SExtractor (Bertin & Arnouts 1996) on the ACS z-band image, and have found $PA_{phot} \sim 22 \pm 2$ deg (relative to the right side of Fig. 2, counterclockwise). This is very close to the outer dynamical axis (simply defined as the line connecting V_{max} and V_{min}), with $PA_{kin} \sim 18 \pm 9$ deg. We also note a progressive twist in the isovelocity contours, which might indicate a possible warp in the gas disk. Warps are a common feature of HI disks, although at much larger radii (Binney 1992), but are also observed in a very large fraction of stellar disks (Reshetnikov & Combes 1998). Interestingly, Schwarzkopf & Dettmar (2001) found that tidal interactions and minor mergers contribute considerably to the formation and size of warps. However, we find that spatial resolution issues could account for at least part of this twist. Of note, using the IRAF ellipse task, we find a progressive twist of the (z-band) isophotal ellipses between R_{half} and $2R_{half}$, from ~ 30 deg to ~ 20 deg, respectively. Thus, it remains unclear whether or not this twist truly reflects a warp.

At the GIRAFFE spatial resolution (seeing ~ 0.8 arcsec), undisturbed rotating disks should present a peak in their σ -maps, close to the dynamical center. Indeed, the velocity dispersion

¹ http://archive.stsci.edu/pub/hlsp/goods/v1/h_goods_v1.0_rdm.html#4.0

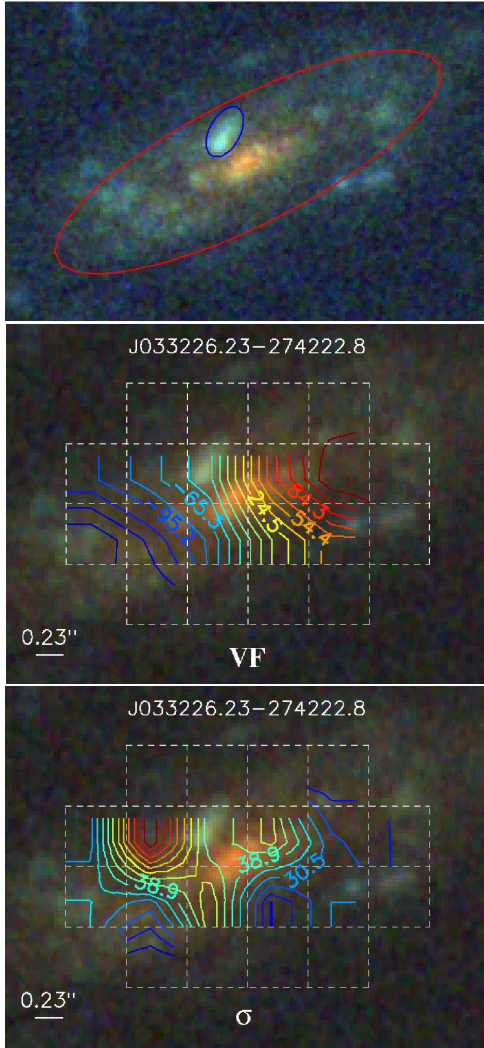


Fig. 2. *Top panel:* Closer view of J033226.23-274222.8, which has been rotated to be aligned with the GIRAFFE IFU compared to Fig. 1 (contrast has been optimized by hand). The two elliptical apertures used to estimate the stellar mass ratio between the two galaxies are shown in red for the main progenitor, and in blue for the infalling satellite (see § 4.1). *Middle and bottom panels:* Three bands ACS imaging of J033226.23-274222.8, superimposed with the GIRAFFE velocity field (*middle*), or σ -map (*bottom*). The IFU bundle is overlaid in white dashed lines (0.52 arcsec/pix). Note that a S/N=3 threshold is used to limit measurement uncertainties, which explains why kinematical data do not extend over the whole IFU FoV. Contours range approximately from -155 to 130 km/s with a 15 km/s spacing for the VF, and from 14 to 73 km/s with a 4 km/s spacing for the velocity dispersion map.

measured within one GIRAFFE pixel is the convolution between random motions occurring at small spatial scales, and integrated larger scale motions (rotation) which enlarge the emission line profile. Thus, because of the rising part of the rotation curve around the dynamical center, one expects this region to be dominated by the latter. This translates into a peak in the 2D σ -maps of regular rotating disks, located at the center of rotation (Yang et al. 2007). In the case of J033226.23-274222.8, because of the relatively coarse spatial resolution of GIRAFFE, this central peak is spread over two pixels located around the red bulge (see Fig. 2).

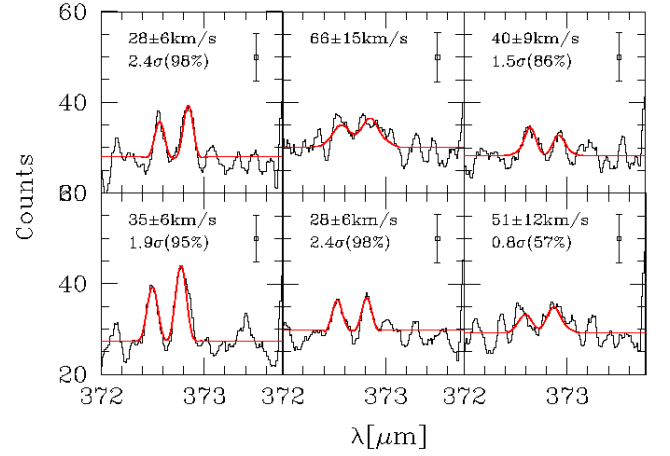


Fig. 3. GIRAFFE spectra in the IFU pixels surrounding the peak of the σ map (here in the upper-middle panel). Observed sky-subtracted spectra are plotted in black, while the [OII] emission line fits are in red. The corresponding σ and its associated uncertainty are indicated in each pixel, together with the level of significance of the difference with the σ peak. The probability that the difference is significant is indicated into parenthesis (see text). Spectra have been smoothed for ease of visualization. A typical 1- σ error bar due to photon noise is represented in each upper-right corner.

As noted in the introduction, 25% of the GIRAFFE galaxies show regular rotating VFs but do not show such a σ peak at their dynamical center. Instead, the σ peak is found in the disk region, as observed in the case of J033226.23-274222.8, with a peak of 66 km/s located one GIRAFFE pixel left of the infalling satellite. In Fig. 3, we plot the corresponding IFU spectrum and those in adjacent pixels. One can derive the level of significance of the difference between the peak and the dispersion measured in the neighbor pixels using $(\sigma_{\text{peak}} - \sigma_{\text{neighbor}}) / \sqrt{(\delta\sigma_{\text{peak}}^2 + \delta\sigma_{\text{neighbor}}^2)}$, where $\delta\sigma$ is the uncertainty associated with σ . In doing so, we assume a one-sided Gaussian distribution for the relative uncertainty on the σ measurement (see Yang et al. 2007). A high level of significance is found for the difference between the peak and all the surrounding pixels. We also do not see any special variation of the standard deviation of the fit in this pixel compared with neighboring ones. Thus, it is unlikely that the σ peak results from artefacts due to S/N effects or to sky residuals.

Such an offset between the gas σ peak and the stellar mass distribution of the infalling satellite could simply result from a decoupling between stars and gas, as observed in numerical simulations of such interactions (e.g., Hernquist & Mihos 1995). In this context, the σ peak would correspond to the location of the shock between the gas stripped away from the infalling satellite and the gas of the main progenitor, which would lead to an increase of σ , as observed numerically (e.g., Robertson et al. 2006). Noteworthy, simulations of giant molecular clouds show how shocks can generate a velocity dispersion $\sigma[\text{km/s}] \sim L[\text{pc}]^{1/2}$ (Bonnell et al. 2006), where L is the spatial scale of interest (i.e., at which σ is measured). Assuming that this relation can be extrapolated to galactic scales, one finds that at the scale of a GIRAFFE pixel ($\sim 3.6 \text{ kpc}$), the shock-generated σ would be $\sim 60 \text{ km/s}$, which is consistent with the peak value.

4. SFR and mass estimates

4.1. Stellar and dynamical mass

In Puech et al. (2007b), we derive a rotational velocity $V_{rot} = 200 \text{ km/s}$, corrected for inclination and spatial resolution effects. Following Puech et al. (2007a), we estimate the V/σ ratio in the disk to be $\sim 8.8 \pm 1.8$, compatible with a thin late-type rotating disk (see also Fathi et al. 2007). We can thus assume full rotational support, which leads to a total dynamical mass within the optical radius ($\sim 2R_{half}$), $\text{Log}(M_{dyn}/M_{\odot}) \sim 11$. It is however not possible to derive a direct estimate of M_{dyn} for the accreted object because the σ peak probably traces shock heating rather than gravitational motions, since it does not correspond to the underlying mass distribution (see discussion in Colina et al. 2005).

On the other hand, it is possible to derive a rough estimate of the stellar mass ratio between the two progenitors, by defining two elliptical apertures on the z-band image, the reddest image at our disposal. For the main progenitor, we used directly the elliptical aperture returned by SExtractor. For the infalling galaxy, we defined an elliptical aperture by hand, guided by the B-V-z image (see Fig. 2). We then estimated the stellar mass ratio between the two progenitors by simply deriving the ratio between the counts obtained within the respective apertures. Finally, we corrected this by the V-z color difference between the two progenitors (~ 0.24), which we approximate to the u-g color at rest. Using the stellar mass calibration given by Bell et al. (2003), we find a final mass ratio of $\sim 1:18$.

Following Ravikumar et al. (2007), the stellar mass for the two progenitors is $\text{Log}(M_{stellar}/M_{\odot}) = 10.72$, which leads to $\text{Log}(M_{stellar}/M_{\odot}) \sim 10.7$ and $\text{Log}(M_{stellar}/M_{\odot}) = 9.5$ for the main and minor progenitors respectively. Of note, this correspond for the main progenitor to a $M_{stellar}/M_{dyn} \sim 0.5$, which is in the range of values measured by Conselice et al. (2005). Moreover, J033226.23-274222.8 follows the relation $M_{dyn} = 10^{-2.4} M_{stellar}^{1.25}$ found by Rettura et al. (2006): assuming that this relation can be extended to galaxies having $\text{Log}(M_{stellar}/M_{\odot}) \leq 10$, a stellar mass ratio of 1:18 leads to a dynamical mass ratio of $\sim 1:37$. We are thus quite confident that we are in the presence of the accretion of a relatively small satellite.

4.2. Star formation rate

We first use the $24\mu\text{m}$ MIPS DR-3 data to derive the dust-obscured SFR_{IR} . At $z=0.6679$, this flux roughly corresponds to a rest-frame $15\mu\text{m}$ flux: we can thus use the Chary & Elbaz (2001) calibration to derive the total IR luminosity L_{IR} , and then use the classical Kennicutt (1998) calibration between L_{IR} and SFR_{IR} . We find $\text{SFR}_{IR} = 17.5 M_{\odot}/\text{yr}$, corresponding to $f_{24\mu\text{m}} = 91.7 \mu\text{Jy}$. To determine the unobscured SFR_{UV} , we used the UV calibration of Kennicutt (1998), using the rest-frame 2800\AA luminosity. We find $M_{2800} = -20.12$, leading to $\text{SFR}_{UV} = 3.2 M_{\odot}/\text{yr}$. We thus find a total $\text{SFR}_{tot} = \text{SFR}_{UV} + \text{SFR}_{IR} \sim 20.7 M_{\odot}/\text{yr}$. Assuming a constant SFR during the disk build-up, and neglecting the contribution of the bulge to the total stellar mass ($B/T=0.05$), we can roughly estimate a timescale for the formation of the disk using $M_{stellar}/\text{SFR}_{tot} \sim 2.5 \text{ Gyr}$.

We used the B-z colormap to define star-bursting regions in the disk and the satellite as those having $B-z < 1$ (Neichel et al. 2007). We find that the satellite star-bursting regions represent $\sim 15\%$ of the B-band flux located in all star-bursting regions of the disk (satellite excluded). Moreover, the ratio between the obscured and unobscured SFR is ~ 5.5 , which is lower than the me-

dian ratio found in $0.4 \leq z \leq 1$ star-burst galaxies (~ 13 , see, e.g., Hammer et al. 2005): assuming there are no completely dust-obscured star forming regions, this leads us to a contribution of HII star-bursting regions to SFR_{tot} of $\sim 85\%$, corresponding to $\sim 17.6 M_{\odot}/\text{yr}$. Therefore, the SFR enhancement due to the satellite would be $\sim 3.1 M_{\odot}/\text{yr}$, which is comparable to what is found in observations (Woods & Geller 2007).

5. Conclusion

In this *letter*, we have presented the first detection of a minor merger at high redshift ($z=0.6679$). Using ACS imaging, we identified an infalling satellite onto a late-type spiral. Gas kinematics reveals a velocity field with no large-scale perturbations, except a twist in the isovelocities which might indicate a possible warp of the gaseous disk. Such a warp is also seen in the stellar disk, using photometric isophotes. The gas σ -map shows a peak off-centered from the dynamical center, and close to the infalling satellite. Such a peak cannot be attributed to rotation and is interpreted as the signature of shock-heated gas during the collision. We derive a total $\text{SFR} \sim 21 M_{\odot}/\text{yr}$ and a rough stellar mass ratio estimate $\sim 1:18$, in agreement with this kind of events. Therefore, J033226.23-274222.8 seems to be the first detection of a minor merger at $z \sim 0.6$, and more generally at high redshift. This study demonstrates that using 3D spectroscopy appears to be a promising tool to identify minor mergers, both in nearby and distant galaxies. Finally, minor mergers are a good candidate to explain the kinematics observed in perturbed rotating galaxies, which account for 25% of emission line intermediate mass galaxies at $z \sim 0.6$.

Acknowledgements. The authors wish to thank an anonymous referee for useful comments and suggestions.

References

- Bell, E.F., McIntosh, D.H., Katz, N., & Weinberg, M.D. 2003, *ApJSS*, 149, 289
- Bertin, E., & Arnouts, S. 1996, *A&ASS*, 117, 393
- Binney, J. 1992, *ARA&A*, 20, 51
- Bonnell, I.A., Dobbs, C.L., Robitaille, T.P., & Pringle, J.E. 2006, *MNRAS*, 365, 37
- Bournaud, F., Jog, C.J., & Combes, F. 2005, *A*, 437, 69
- Chary, R., Elbaz, D. 2001, *ApJ*, 556, 562
- Colina, L., Arribas, S., Monreal-Ibero, A., *ApJ*, 621, 725
- Conselice, C. J., Bundy, K., Ellis, R. S., Brichmann, J., Vogt, N. P., & Phillips, A. C. 2005, *ApJ*, 628, 160
- Fathi, K., Beckman, J.E., Zurita, A., et al. 2007, *A*, 466, 905
- Flores, H., Hammer, F., Puech, M., Amram, P., & Balkowski, C. 2006, *A&A*, 455, 107
- Förster-Schreiber, N.M., Genzel, R., Lehnert, M.D., et al. 2006, *ApJ*, 645, 1062
- Guo, Q., & White, S. 2007, *astro-ph/0708.1814*
- Hammer, F., Flores, H., Elbaz, D., Zheng, X. Z., Liang, Y. C., & Cesarsky, C. 2005, *A&A*, 430, 115
- Hernquist, L., & Mihos, J. 1995, *ApJ*, 448, 41
- Kennicutt, R. 1998, *ARA&A*, 36, 189
- Khochfar, S., Silk, J. 2006, *MNRAS*, 370, 902
- Laine, S., & Heller, C. 1999, *MNRAS*, 308, 557
- Law, D.R., Steidel, C.C., Erb, D.K., et al. 2007, *ApJ*, accepted, *astro-ph/0707.3634*
- Neichel, B., et al. 2007, *A&A*, in prep.
- Pasquini, L., Castillo, R., Dekker, H., et al. 2004, *SPIE Proc.*, 5492, 136
- Puech, M., Hammer, F., Flores, H., Östlin, G., & Marquart, T. 2006b, *A&A*, 455, 119
- Puech, M., Hammer, F., Lehnert, M. D., & Flores, H. 2007a, *A&A*, 466, 83
- Puech, M., Flores, H., Hammer, F., et al. 2007a, *A&A*, in prep.
- Ravikumar, C. D., et al. 2007, *A&A*, 465, 1099
- Reshetnikov, V., & Combes, F. 1998, *A*, 337, 9
- Rettura, A., Rosati, P., Strazzullo, V., et al. 2006, *A*, 458, 717
- Robertson, B., Bullock, J. S., Cox, T. J., Di Matteo, T., Hernquist, L., Springel, V., & Yoshida, N. 2006, *ApJ*, 645, 986

- Schwarzkopf, U., & Dettmar, R.-J. 2000, *â*, 361, 451
Schwarzkopf, U., & Dettmar, R.-J. 2001, *â*, 373, 402
Toth, G., & Ostriker, J. 1992, *ApJ*, 389, 5
Velazquez, H., & White, S. 1999, *MNRAS*, 304, 254
Walker, I., Mihos, J., & Hernquist, L. 1996, *ApJ*, 460, 121
Woods, D., Geller, M., & Barton, E. 2006, *AJ*, 132, 197
Woods, D., & Geller, M. 2007, *AJ*, 134, 527
Yang, Y., Flores, H., Hammer, F., et al. 2007, *A&A*, submitted
Yoachim, P., & Dalcanton, J. 2006, *ApJ*, 131, 226
Younger, J., Cox, T.J., Seth, A., & Hernquist, L. 2007, *ApJ*, accepted, astro-ph/0707.4481